Electronic Supplementary Material (ESI) for Sustainable Energy & Fuels.

Supporting Information for:

Performance and Failure Modes for Si Anodes Patterned with Thin Film Ni Catalyst Islands for Water Oxidation

Ke Sun[1], Nicole L. Ritzert[2,3], Jimmy John[1], Haiyan Tan[2,3], William G. Hale[4], Jingjing Jiang[5], Ivan Moreno-Hernandez[1], Kimberly M. Papadantonakis[1], Thomas P. Moffat[3], Bruce S. Brunschwig[6], and Nathan S. Lewis[1,6*]

[1]Division of Chemistry and Chemical Engineering, California Institute of Technology, 1200 E. California Blvd., Pasadena, CA 91125, USA

[2]Theiss Research, 7411 Eads Ave., La Jolla, California 92037, USA

[3]National Institute of Standards and Technology, Material Measurement Laboratory, 100 Bureau Dr., Gaithersburg, MD 20899, USA

[4]Department of Chemistry, University of Southampton, Southampton, Hampshire SO17 1BJ, UK

[5]Division of Engineering and Applied Sciences, California Institute of Technology, 1200 E. California Blvd., Pasadena, CA 91125, USA

[6]Beckman Institute Molecular Materials Research Center, California Institute of Technology, Pasadena, 1200 E. California Blvd, CA 91125, USA

*Correspondence to: nslewis@caltech.edu

Supporting Experimental Details

XPS characterization:

Two p^+-Si(111)|NiμE$_{35.7\%}$ samples were examined by XPS. Measurements were performed with a Kratos AXIS Ultra DLD with a monochromatic Al Kα source. The spectrometer was calibrated to Au $4f_{7/2}$ 84.0 eV, Ag $3d_{5/2}$ 368.2 eV, and Ag MNN 1128.9 eV signals, and all spectra were collected at a 90° take-off angle. Spectra were fit using Casa XPS software v. 2.3.15 with the peaks modeled with a Voigt function (70% Gaussian-30% Lorentizian) and a Shirley background correction. Ni $2p_{3/2}$ spectra were fit using a fully constrained parameter set based on the weighted sum of the convolved peak shapes that have been determined previously for $Ni(OH)_2$, NiO and Ni standards.[1, 2] The peak binding energy of the NiO, $Ni(OH)_2$ and Ni envelope was freely adjusted during fitting, while the separation of individual peaks and their relative intensity within each envelope were fixed. A reasonable fit was obtained considering the signal-to-noise ratio and the limited nature of the data set examined. Comparison between the intensity of the fitted NiO, $Ni(OH)_2$ and Ni envelopes allowed the overlayer thickness, d_{oxNi}, to be estimated based on the density of Ni in the respective phases, N_{m}, N_{ox}, N_{hydrox}, with the inelastic mean free path for photoelectrons in the overlayer being the weighted average, $\lambda_{\mathrm{ox:hydro}}$, of that for NiO, and $Ni(OH)_2$.[1]

$$d_{oxNi} = \lambda_{ox:hydro} ln\left(\frac{N_m \lambda_m (I_{ox} + I_{hydrox})}{N_{ox:hydro} \lambda_{ox:hydrox} I_m} + 1\right) \qquad \text{(s1)}$$

For the Si 2p spectra, SiO_2 was clearly resolved from elemental Si, although sub-stoichiometric species were also evident. Fitting was constrained by the $2p_{3/2}/2p_{1/2}$ spin-orbit area ratio of 2, a fixed FWHM for each species, along with the binding energy of the sub-stoichiometric oxide states, with the exception of "Si_2O" which was free to adjust. Si-OH and related species were not explicitly considered although they likely play a role in the perturbation of the various

assignments. Extracting accurate and precise film-thickness values, d_{oxSi}, is complex. Consequently, a simple overlayer model was used herein to parameterize the film thickness based on the inelastic mean free path, λ, of 3.14 +/- 0.31 nm for Si 2p photoelectrons and a derived ratio, R_o, of 0.87 for the bulk intensity for pure SiO_2 and Si subject to Al Kα excitation.[3] From the measured ratio of the oxide to the elemental peak intensity, R_{meas}, the oxide thickness was given by:

$$d_{ox} = \lambda * \ln\left(1 + \frac{R_{meas}}{R_o}\right) \qquad \text{(s2)}$$

Photocurrent density from integration against the AM 1.5G spectrum:

The integrated photocurrent density obtained by convoluting the measured external quantum yield data with the spectral distribution of the standard AM 1.5G spectrum was calculated using the following equation:

$$J = \int_{\lambda=350}^{\lambda} {}^{q}/_{hc}\Phi_{ext}(\lambda)\cdot\Gamma(\lambda)\cdot\lambda\cdot d\lambda \approx \int_{\lambda=350}^{\lambda} {}^{\Phi_{ext}(\lambda)\cdot\lambda}/_{1240}\cdot\Gamma(\lambda)\cdot d\lambda \qquad \text{(s3)}$$

where J is the integrated photocurrent density in A m^{-2}, q is the unsigned charge on an electron, h is Planck's constant (6.63×10^{-34} J s), c is the speed of light (2.998×10^{8} m s^{-1}), Φ_{ext} is the measured external quantum yield, Γ is the irradiance in W m^{-2} nm^{-1}, λ is the light wavelength in nm, 1240 is in W nm A^{-1}, and $\Phi_{ext}\cdot\lambda/1240$ is the responsivity in A W^{-1}.

Calculation of the branching ratio for currents:

The total charge needed to fully dissolve the Si underneath the catalyst islands (step 4 in Figure 9c) was calculated by approximating the dissolved volume of Si as hemispheres beneath the catalyst islands:

$$Q_{SOR} = 4 \times \frac{1}{2} \times \frac{4}{3}\pi r^3 \times \frac{ff}{\pi r^2} \times \rho_a \times e \quad \text{(s4)}$$

Q_{SOR} is the charge density for silicon oxidation reactions in C cm^{-2}, r is the radius of the catalyst islands in cm, ff is the filling fraction, ρ_a is the atomic density in cm^{-3} (5×10^{22} cm^{-3}), and e is the elementary charge (1.6×10^{-19} C). The number of electrons considered is 4.

The total charge passed before failure can be calculated from equation s5:

$$Q_{total} = J \times t \times 3.6 \quad \text{(s5)}$$

Q_{total} is the total charge density in C cm^{-2} passed during the stability test, J is the photocurrent density in mA cm^{-2} used in stability measurement, and t is operational lifetime in h.

The current-branching ratio is given by:

$$\frac{J_{SOR}}{J_{OER}} \approx \frac{Q_{SOR}}{Q_{total}} = 0.58\frac{r \cdot ff}{J \cdot t} = 6 \times 10^{-4} \quad \text{(s6)}$$

where J and t in the calculation are based on data shown in Figure 2C.

Assuming that this process represents the only degradation mechanism, the operational lifetime of Si devices based on this design can be determined by:

$$t = \frac{966 \times r}{J_{cat}} \quad \text{(s7)}$$

where J_{Cat} is the current density in mA cm^{-2} normalized to the filling fraction of the catalyst islands, which equals *J/ff*.

Supporting Figures

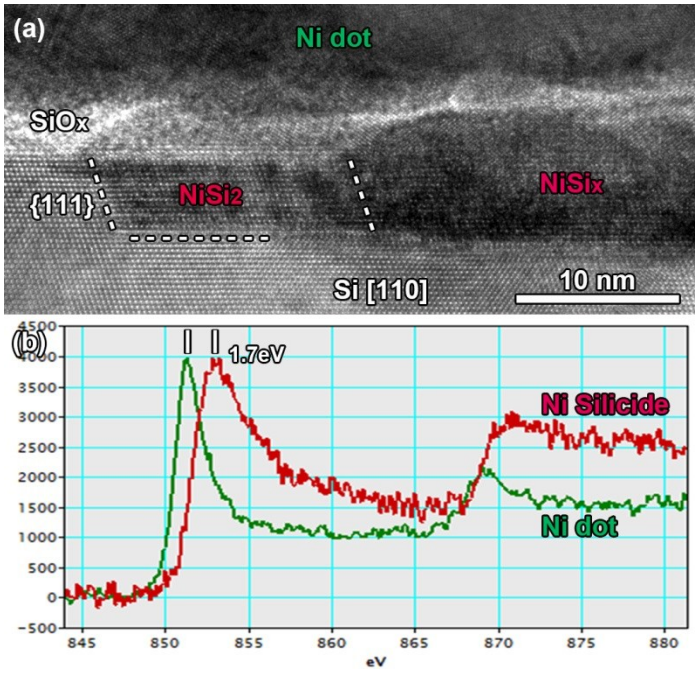

Figure S1. (a) High-resolution transmission electron micrograph of the interface between the Ni dots and the Si substrate along the Si[110] zone axis. $NiSi_2$ shows a facet growth with epitaxial relationship with the Si substrate. Another $NiSi_x$ island is also observed with thicker size and unclear crystal structure. (b) Electron-Energy-Loss Spectra (EELS) of the Ni L edge (after power-law background removal) collected in the crystalline interfacial region (red curve) and in the polycrystalline Ni region (green curve). The spectra were precisely aligned to the zero-loss peak acquired in rapid succession. The Ni edge from Ni silicide shifted 1.7 eV to higher energy-loss compared to that of Ni island layer.

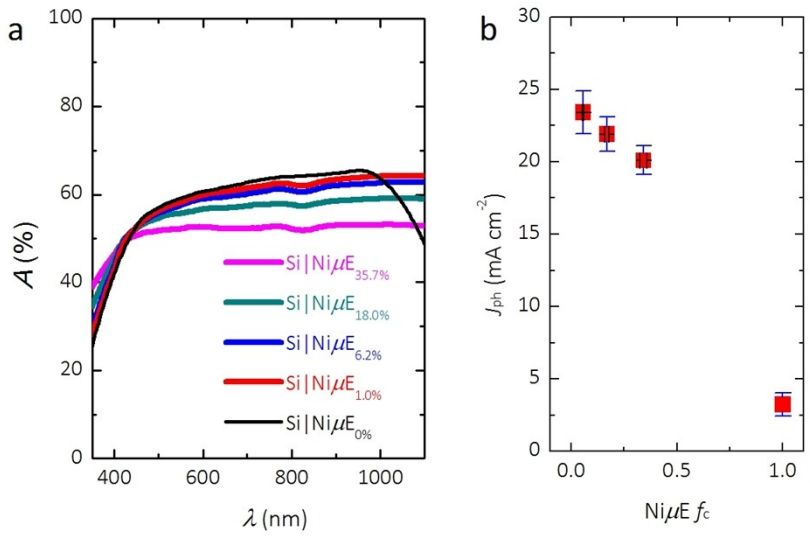

Figure S2. a) Absorptance and b) light limited photocurrent calculated by integrating the external quantum efficiencies of Si|NiμEs with disks of 5.6 μm diameter and varying filling fractions (1.0 – 35.7%).

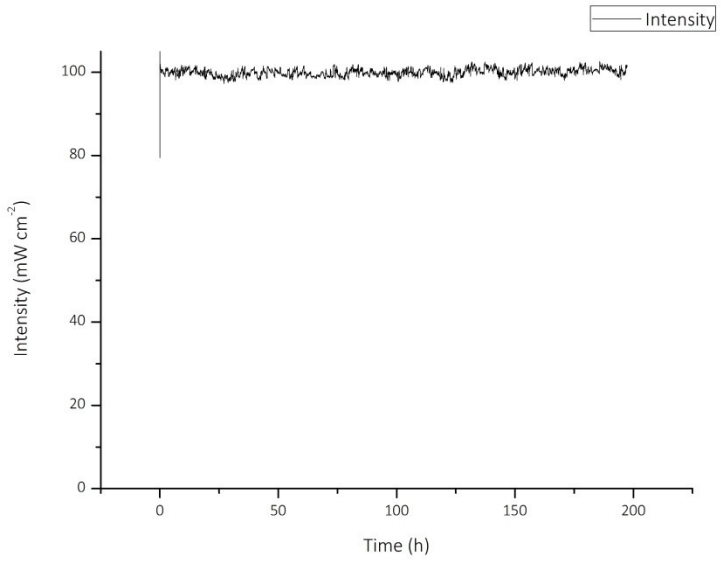

Figure S3. Representative intensity as a function of time for the ELH-type W-halogen lamp used for stability testing, as monitored by a calibrated Si photodiode.

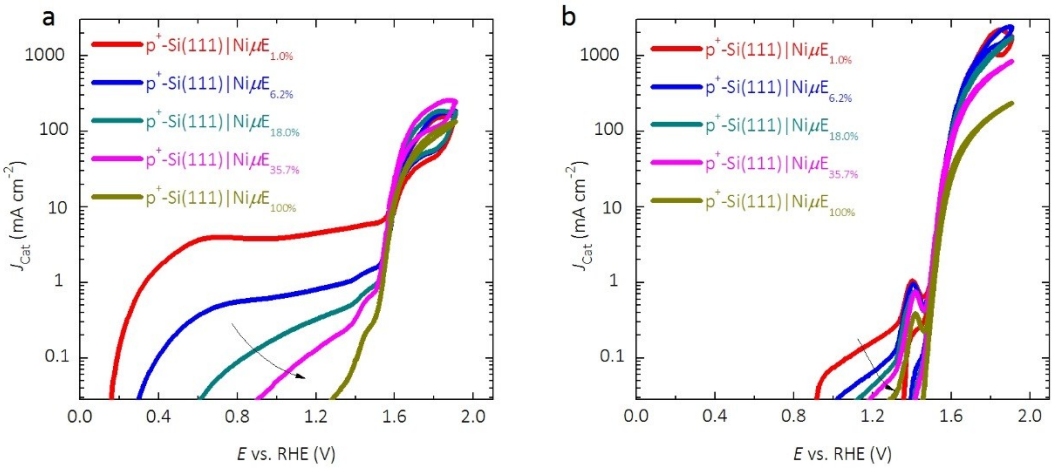

Figure S4. *J-E* behavior for p$^+$-Si(111)|NiμE samples in 1.0 mol L^{-1} KOH(aq) within the potential range from E_{oc} to +1.93 V vs. RHE. J_{Cat} is the current density normalized to the catalyst area. (a) First cycle and (b) tenth cycle at a voltammetric scan rate of 40 mV s^{-1}. The large hysteresis in J_{cat} in the potential range < 1.4V vs. RHE shown in Figure S4a and S4b is caused by the oxidation of exposed Si, the magnitude of which is proportional to the uncovered Si area, while the hysteresis in Figure 3 in the same potential range is caused by the active Ni^{2+} to Ni^{3+} conversion, the magnitude of which is proportional to the Ni island coverage area. At J_{cat} greater than 10 mA cm^{-2} (Figure S4b), J_{cat} decreased with increased island filling fraction, due to an increase in the concentration overpotential. Due to radial diffusion, the performance of the patterned electrocatalyst film showed a smaller concentration-overpotential loss than Ni films, and was independent of the thickness of the hydrodynamic boundary layer, in contrast to the situation for Ni films.

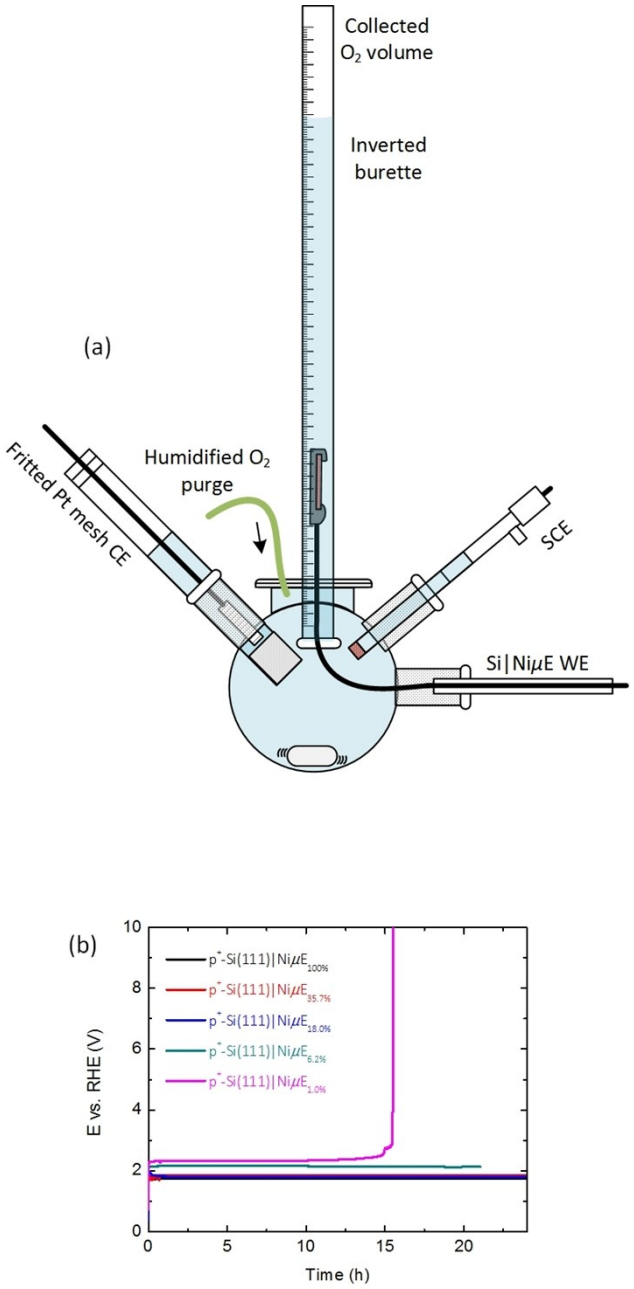

Figure S5.a) Faradaic efficiency measurement setup and b) potential profiles of p^+-Si(111)|NiμEs with different filling fractions of Ni catalyst islands during the measurement described in **Figure 4**. The potentials were not corrected for resistance losses from the measurement setup. Anodic potentials for all electrodes tested were typically stabilized after 2 hours of operation during the Faradaic efficiency measurement. The stabilized potentials that

were required to drive a constant current density of 10 mA cm^{-2} were 2.33, 2.17, 1.86, 1.79 and 1.75 V vs. RHE for electrodes with filling fractions of 1.0%, 6.2%, 18.0%, 35.7% and 100%, respectively.

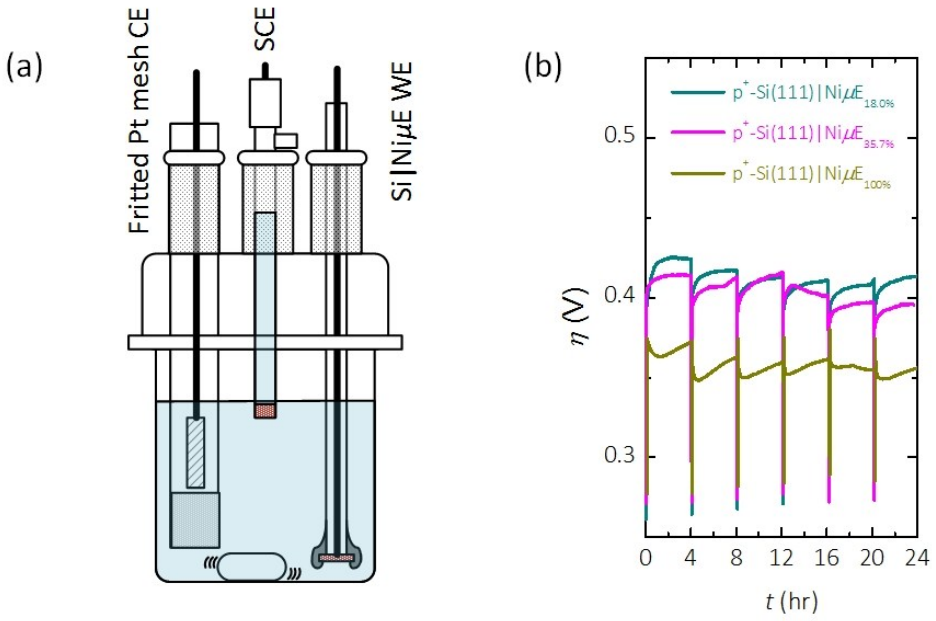

Figure S6. a) Electrochemical measurement setup and potential profiles of p^+-Si(111)|NiμEs with filling fractions of 18.0%, 35.7% and 100% operating at a constant geometric current density of 30 mA cm^{-2} during a 24-h stability measurement. The stability measurement was interrupted every 4 h to collect data for ten cyclic voltammetry cycles.

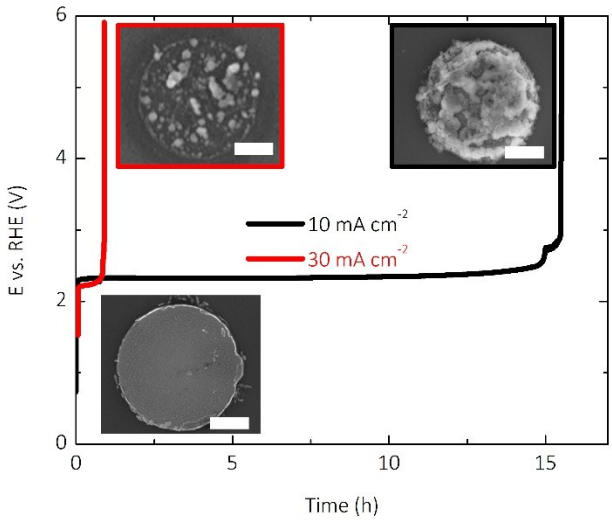

Figure S7. Comparison of the potential profiles of p^+-Si(111)|NiμE$_{1.0\%}$ at 10 mA cm^{-2} (black curve) and 30 mA cm^{-2} (red curve). Insets are SEM images collected on an as-prepared p^+-Si(111)|NiμE$_{1.0\%}$ (lower left corner) electrode and on the identical sample removed from solution after failure. Scale bars in the SEM images are 2 μm. The higher potential required to sustain a lower current density (10 mA cm^{-2}, black curve, measured using setup in **Figure S5a**) compared to that to sustain a higher current density (30 mA cm^{-2}, red curve, measured using setup in **Figure S6a**) is likely caused by the larger uncompensated resistance loss in the set-up used for the faradaic efficiency measurements.

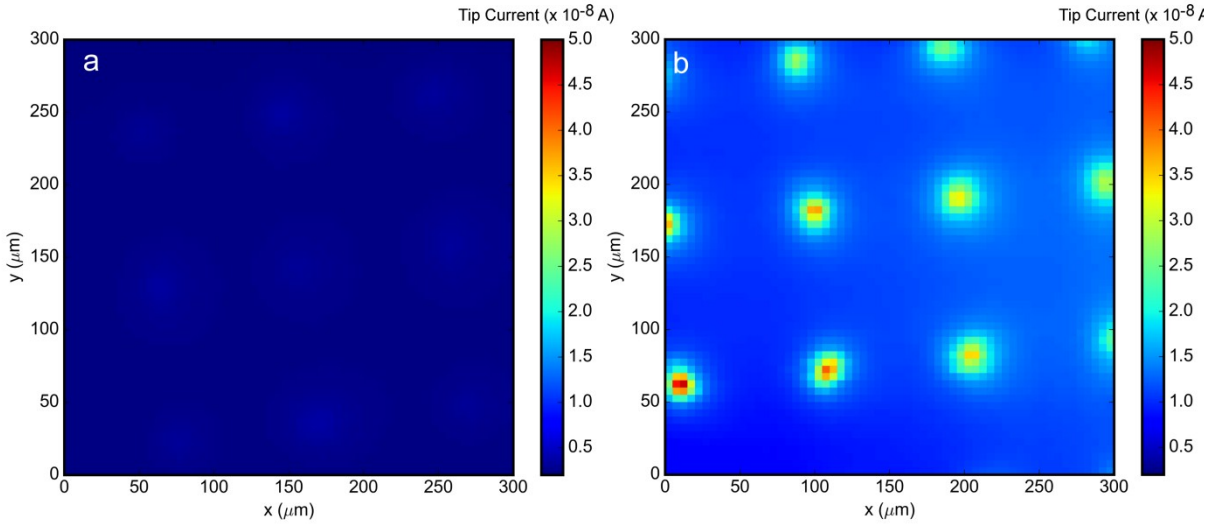

Figure S8. SECM images of p^+-Si(111)|Ni$\mu E_{1.0\%}$ in 0.88 mol L^{-1} KOH (a) before and (b) after polishing the tip electrode. The Pt tip (10 μm in diameter) and substrate potentials were poised at +0.45 V and +1.85 V vs. RHE, respectively. The tip-substrate separation was 6 μm and the scan rate was 100 μm s^{-1}.

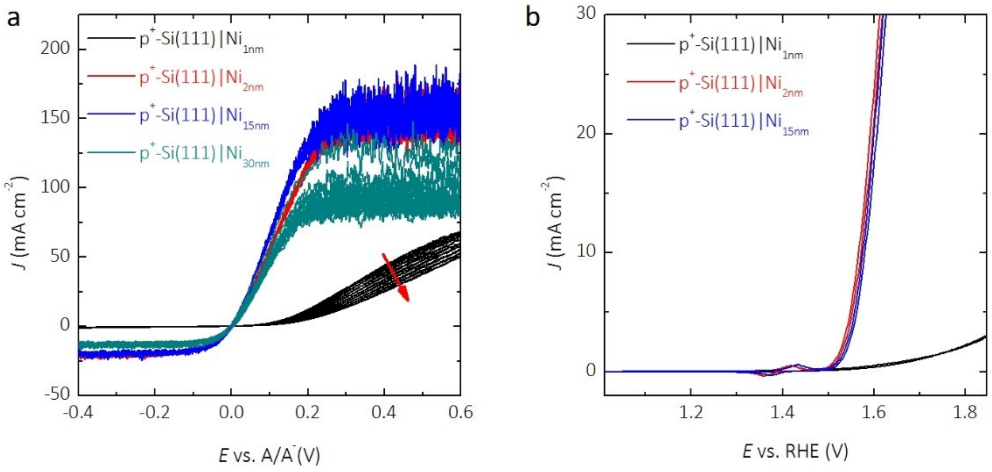

Figure S9. (a) *J-E* behavior of p^+-Si(111) substrates with varying Ni film thickness when the electrodes were in contact with 50 mmol L^{-1} $K_3Fe(CN)_6$, 350 mmol L^{-1} $K_4Fe(CN)_6$, and 1.0 mol L^{-1} KCl). (b) *J-E* behavior at 40 mV s^{-1} scan rate of p^+-Si(111)|Ni films in contact with 1.0 mol L^{-1} KOH.

References:

1. M. C. Biesinger, B. P. Payne, L. W. M. Lau, A. Gerson and R. S. C. Smart, *Surf. Interface Anal.*, 2009, **41**, 324-332.

2. A. P. Grosvenor, M. C. Biesinger, R. S. C. Smart and N. S. McIntyre, *Surf. Sci.*, 2006, **600**, 1771-1779.

3. M. P. Seah and S. J. Spencer, *Surf. Interface Anal.*, 2002, **33**, 640-652.